Toxicology and Applied Pharmacology 273 (2013) 289–297

Contents lists available at ScienceDirect

Toxicology and Applied Pharmacology

journal homepage: www.elsevier.com/locate/ytaap

Zinc ferrite nanoparticles activate *IL-1b*, *NFKB1*, *CCL21* and *NOS2* signaling to induce mitochondrial dependent intrinsic apoptotic pathway in WISH cells

Quaiser Saquib [a,b], Abdulaziz A. Al-Khedhairy [a,b], Javed Ahmad [a,b], Maqsood A. Siddiqui [a,b], Sourabh Dwivedi [a,b], Shams T. Khan [a,b], Javed Musarrat [b,c,*]

[a] Department of Zoology, College of Science, King Saud University, P.O. Box 2455, Riyadh 11451, Saudi Arabia
[b] Chair for DNA Research, Department of Zoology, College of Science, King Saud University, P.O. Box 2455, Riyadh 11451, Saudi Arabia
[c] Department of Agricultural Microbiology, Faculty of Agricultural Sciences, Aligarh Muslim University, Aligarh 202002, U.P., India

ARTICLE INFO

Article history:
Received 9 July 2013
Revised 28 August 2013
Accepted 3 September 2013
Available online 10 September 2013

Keywords:
Zinc ferrite
Oxidative stress
DNA damage
Nanoparticles
Apoptosis
Cytotoxicity

ABSTRACT

The present study has demonstrated the translocation of zinc ferrite nanoparticles ($ZnFe_2O_4$-NPs) into the cytoplasm of human amnion epithelial (WISH) cells, and the ensuing cytotoxicity and genetic damage. The results suggested that *in situ* NPs induced oxidative stress, alterations in cellular membrane and DNA strand breaks. The [3-(4,5-dimethylthiazol-2-yl)-2,5-diphenyltetrazolium bromide] (MTT) and neutral red uptake (NRU) cytotoxicity assays indicated 64.48 ± 1.6% and 50.73 ± 2.1% reduction in cell viability with 100 μg/ml of $ZnFe_2O_4$-NPs exposure. The treated WISH cells exhibited 1.2-fold higher ROS level with 0.9-fold decline in membrane potential ($\Delta\Psi m$) and 7.4-fold higher DNA damage after 48 h of $ZnFe_2O_4$-NPs treatment. Real-time PCR (qPCR) analysis of *p53*, *CASP* 3 (caspase-3), and *bax* genes revealed 5.3, 1.6, and 14.9-fold upregulation, and 0.18-fold down regulation of *bcl 2* gene *vis-à-vis* untreated control. RT^2 Profiler™ PCR array data elucidated differential up-regulation of mRNA transcripts of *IL-1b*, *NFKB1*, *NOS2* and *CCL21* genes in the range of 1.5 to 3.7-folds. The flow cytometry based cell cycle analysis suggested the transfer of 15.2 ± 2.1% ($p < 0.01$) population of $ZnFe_2O_4$-NPs (100 μg/ml) treated cells into apoptotic phase through intrinsic pathway. Over all, the data revealed the potential of $ZnFe_2O_4$-NPs to induce cellular and genetic toxicity in cells of placental origin. Thus, the significant ROS production, reduction in $\Delta\Psi m$, DNA damage, and activation of genes linked to inflammation, oxidative stress, proliferation, DNA damage and repair could serve as the predictive toxicity and stress markers for ecotoxicological assessment of $ZnFe_2O_4$-NPs induced cellular and genetic damage.

Introduction

Certain *in vivo* studies have demonstrated that nanoparticles (NPs) exposure can provoke inflammatory responses, oxidative stress, myocardial infarction and thrombosis (Kumar, 2006). They can also alter the permeability of blood brain barrier and re-translocate from the site of deposition to other parts of the body *via* circulatory or lymphatic system (AshaRani et al., 2009; Kumar, 2006; Zhao and Nalwa, 2007). A majority of NPs get internalized in cells through phagocytosis, macropinocytosis, receptor-mediated endocytosis, and passive penetration (Tantra and Knight, 2011; Zhao et al., 2011). Therefore, the importance of their toxicological impact and development of early indicators for detection of possible adverse health effects arising from nanomaterial exposure is strongly realized. In view of unavoidable human exposure to NPs, it seems logical to investigate the cytotoxicity of the metal oxide NPs. One such class of unexplored nanomaterials is spinel ferrite MFe_2O_4 (M = Ni, Co, Mn, Zn, *etc.*), which comprises of immensely popular magnetic materials, with a wide variety of applications in electronic ignition systems, generators, vending machines, medical implants, wrist watches, inductor core, transformer circuits, magnetic sensors and recording equipment, telecommunications, magnetic fluids, microwave absorbers and other high-frequency applications (Prithviraj Swamy et al., 2011). There are limited reports on the toxicity of spinel ferrite NPs. Some earlier studies have suggested that the $NiFe_2O_4$-NPs induced cytotoxicity and apoptosis through ROS generation and oxidative stress *via p53*, survivin, *bax*/*bcl*-2 and caspase pathways (Ahamed et al., 2011; Yin et al., 2005). Also, $CoFe_2O_4$-NPs are reported to interfere with lipid metabolism, and can undergo chemical degradation leading to increased levels of Co in the nuclear region, resulting in cell death (Marmorato et al., 2011). They are also reported to cause embryo toxicity in undifferentiated embryonic stem cell line (ES-D3) (Di Guglielmo et al., 2010). In this study, we have chosen zinc ferrite nanoparticles ($ZnFe_2O_4$-NPs), a lesser investigated class of the spinel ferrites, often used as a contrasting agent in magnetic resonance imaging (MRI) and spintronics devices (Bärcena et al., 2008). $ZnFe_2O_4$-NPs have been reported to induce chromosomal aberration in the meristematic root cells of sunflower (Vochita et al., 2012). Xiao-Feng and Ting (2010) demonstrated increase in the number

* Corresponding author at: Department of Agricultural Microbiology, Faculty of Agricultural Sciences, Aligarh Muslim University, Aligarh 202002, U.P., India. Fax: +91 571 2703516.
E-mail address: musarratj1@yahoo.com (J. Musarrat).

0041-008X/$ – see front matter © 2013 Elsevier Inc. All rights reserved.
http://dx.doi.org/10.1016/j.taap.2013.09.001

of leucocytes and variations in the infrared spectrum of hemoglobin in rats injected with ferrite nanoNi–Zn powders. However, to date, there is no report in literature on the toxic effects of $ZnFe_2O_4$-NPs in human systems. To the best of our understanding, this study for the first time provides a comprehensive information on the cytotoxic and genotoxic potential of $ZnFe_2O_4$-NPs, in cell line of placental origin. There are reports that the WISH (Wistar Institute, Susan Hayflick) cells maintain the similar characteristics of growth, cell morphology, prostaglandin production, and susceptibility to apoptotic agents, as the primary amnion cells (Lundgren et al., 1997; Moore et al., 2002). Perhaps, the stability of these cells makes them more useful for studies that the primary cultures of amnion cells will not tolerate (Kumar et al., 2004). Therefore, the cultured amniotic WISH cells were chosen as an *in vitro* test model, to assess the effects of $ZnFe_2O_4$-NPs on the (i) cell viability and internalization of NPs, (ii) intracellular ROS production and dissipation of mitochondrial membrane potential ($\Delta\Psi m$), (iii) induction of DNA strand breaks, (iv) cell cycle alterations, (v) transcriptional and translational expression of some apoptosis related genes (*p53*, *bax*, *bcl* 2 and *caspase* 3), and (vi) transcriptomics of a set of 84 human stress and toxicity pathway related genes.

Methods

Characterization of $ZnFe_2O_4$-NPs. $ZnFe_2O_4$-NPs (Cat # 633844), >99% trace metals basis, particle size <100 nm (BET) were purchased from Sigma Chemical Company (St. Louis, MO, USA). Homogenous stock suspension of 2 mg/ml $ZnFe_2O_4$-NPs was prepared in deionized ultrapure water by sonication for 20 min at 40 W. Stock suspension was then instantly diluted both in the ultrapure water and RPMI cell culture medium just before the experiments. Commercially available $ZnFe_2O_4$-NPs were further characterized by transmission electron microscopy (TEM) and atomic force microscopy (AFM) analyses. Also, the primary and secondary sizes of $ZnFe_2O_4$-NPs in aqueous suspension, and zeta (ζ)-potential were determined by measuring dynamic light scattering (DLS) by use of a ZetaSizer-HT (Malvern, UK), as described earlier (Saquib et al., 2012a; Dwivedi et al., 2013). Briefly, the samples for TEM analysis were prepared by dropping the ultrasonically treated $ZnFe_2O_4$-NP suspension onto a TEM copper grid and dried at room temperature. A total of six TEM samples were prepared, and at least ten micrographs of each were analyzed to determine the sample particle size. TEM was performed on a Field Emission Transmission Electron Microscope (JEM-2100 F, JEOL, Japan) at 200 keV. AFM analysis was performed by running the machine in non-contact tapping mode. The topographical images were obtained at a resonance frequency of 218 kHz by use of AFM (Veeco Instruments, USA), and analyzed through the WSXM software.

Cell culture and $ZnFe_2O_4$-NPs treatment. Human amnion epithelial (WISH) cell line (American Type Culture Collection, accession no. CCL25, Rockville, MD, USA) has been maintained in our laboratory and used for toxicity analysis of $ZnFe_2O_4$-NPs. This cell line was chosen as a model due to its higher stability as compared to the primary cultures of amnion cells (Kumar et al., 2004). Cells were grown in RPMI 1640, supplemented with 10% FBS and antibiotic–antimycotic solution (100×, 1 ml/100 ml of medium) in 5% CO_2 with 95% atmosphere in humidity at 37 °C. Each batch of cells was assessed for cell viability by trypan blue dye exclusion test prior to the experiments and batches showing more than 95% cell viability and passage number between 10 and 15 were used in the study. For $ZnFe_2O_4$-NP treatment, the cells (1×10^4/100 μl/well) in complete RPMI medium were seeded in 96-well plates, and exposed to varying concentrations (20 to 100 μg/ml) of $ZnFe_2O_4$-NPs for 24, 48 and 72 h at 37 °C.

Tetrazolium bromide salt (MTT) and neutral red uptake (NRU) assays. $ZnFe_2O_4$-NP induced cyto- and lysosomal toxicity in WISH cells was assessed by MTT and neutral red dyes, as described previously (Saquib et al., 2012a). In brief, cells (1×10^4) were allowed to adhere for 24 h under high humid environment in 5% CO_2–95% atmospheric air at 37 °C in 96-well culture plates. Cells were exposed to $ZnFe_2O_4$-NPs in the concentration range of 20 to 100 μg/ml for 24, 48 and 72 h. Subsequently, MTT (5 mg/ml stock in PBS) was added in the volume of 10 μl/well in 100 μl of cell suspension, and the plate was incubated for 4 h at 37 °C. At the end of incubation periods, the aqueous medium was carefully aspirated and 200 μl of DMSO was added to each well and mixed gently. The plate was then kept on a rocker shaker for 10 min at room temperature and the purple color developed was read at 550 nm using a microplate reader (Multiskan Ex, Thermo Scientific, Finland). Untreated controls were also run under identical conditions. For the NRU assay, the cells were exposed to $ZnFe_2O_4$-NPs in the concentration range of 20 to 100 μg/ml for 24, 48 and 72 h. Subsequently, the medium was aspirated and cells were washed twice with PBS, and incubated for 3 h in a fresh medium supplemented with neutral red (50 μg/ml). Medium was washed off rapidly with a solution containing 0.5% formaldehyde and 1% calcium chloride. Cells were subjected to further incubation of 20 min at 37 °C in a mixture of acetic acid (1%) and ethanol (50%) to extract the dye, and the absorbance was read at 540 nm on a microplate reader. The values were compared with control set run under identical conditions.

$ZnFe_2O_4$-NPs uptake and reactive oxygen species (ROS) measurement. The TEM analysis of $ZnFe_2O_4$-NPs treated WISH cells for uptake and internalization have been performed following the method described by Saquib et al. (2012a). Briefly, cells (5×10^4) were seeded in 6 well tissue culture plate and allowed to adhere for 24 h in CO_2 incubator at 37 °C. Cells were then exposed to $ZnFe_2O_4$-NPs (100 μg/ml) for 72 h. The untreated and $ZnFe_2O_4$-NPs treated cells were harvested and fixed with 10% glutaraldehyde in 0.1 M cacodylate buffer (pH 7.4) for 20 min. Cells were then suspended in 1% OsO_4 in 0.1 M cacodylate buffer (pH 7.4) for 1 h at 4 °C, followed by 1 h incubation in 2% aqueous uranyl acetate at room temperature. The samples were dehydrated in an ethanol series and embedded in low viscosity araldite resin. Ultrafine sections (60 nm thick) were visualized under high vacuum at 100 kV using a JEOI-1011 electron microscope (JEOL, Tokyo, Japan). The images were captured without any contrast agent to avoid potential artifacts due the deposition of contrast agent crystals.

Intracellular ROS production was determined in WISH cells using a fluorescent probe DCFH-DA, following the method of Saquib et al. (2012a). Quantitative estimation of intracellular ROS were done by use of a Beckman Coulter flow cytometer (Coulter Epics XL/Xl-MCL, USA). In brief, the cells were treated with increasing concentrations of $ZnFe_2O_4$-NPs (20 to 100 μg/ml) for 24, 48 and 72 h and then harvested by spinning at 3000 rpm for 5 min. The pellet was washed twice with cold PBS and resuspended in 500 μl of PBS. Cells were then incubated with DCFH-DA (5 μM) for 60 min at 37 °C in dark. Immediately after incubation, the cells were washed twice with PBS and finally suspended with 500 μl PBS. DCFH-DA stained cells without $ZnFe_2O_4$-NPs treatment were taken as control. The fluorescence was recorded upon excitation at 488 nm. Green fluorescence from 2′,7′-dichlorofluorescein (DCF) was measured in the FL1 Log channel through 525 nm band-pass filter. The qualitative analysis of ROS production was demonstrated by staining the $ZnFe_2O_4$-NPs treated WISH cells with 5 μM of DCFH-DA for 60 min. Images were taken using a fluorescence microscope (Nikon Eclipse 80i, Japan).

Mitochondrial membrane potential ($\Delta\Psi m$) and cell cycle analysis. Mitochondrial membrane potential was determined following the method as described previously (Saquib et al., 2012b). In brief, the control cells and those treated with $ZnFe_2O_4$-NPs (20 to 100 μg/ml) for 24, 48 and 72 h were harvested and centrifuged at 3000 rpm for 5 min. Pellets of cells were washed twice with cold PBS and resuspended in 500 μl of PBS. Cells were further incubated with rhodamine (Rh123) (5 μg/ml) for 60 min at 37 °C in dark with gentle shaking. The membrane potential was calculated as the mean fluorescence intensity (Log FL1 488 nm) of 10,000 cells. Mitochondrial activity was also monitored by observing

changes in fluorescence intensity of the mitochondria-specific dye (Rh123) in WISH cells, as described previously (Saquib et al., 2012b). In brief, the untreated control and those treated with $ZnFe_2O_4$-NPs (20 to 100 μg/ml) for 72 h at 37 °C were stained with 20 μM Rh123 for 1 h at 37 °C, and visualized under a fluorescence microscope (Nikon Eclipse 80i, Japan) at excitation and emission wavelengths of 520 and 590 nm, respectively.

For the cell cycle analysis, WISH cells treated with increasing concentrations of $ZnFe_2O_4$-NPs (20 to 100 μg/ml) for 24, 48 and 72 h were harvested and centrifuged at 3000 rpm for 5 min, and the pellet was washed twice with cold PBS. Cells were then fixed with 500 μl of chilled 70% ice-cold ethanol, and incubated at 4 °C for 1 h. After two successive washes, the cell pellet was again suspended in PBS and stained with propiodium iodide (50 μg/ml) solution containing 0.1% Triton X-100 and 0.5 mg/ml RNase A for 1 h at 37 °C in dark. The red fluorescence of 10,000 events of propiodium iodide stained cells were acquired in FL4 Log channel through a 675 nm band-pass filter using flow cytometer. The data were analyzed excluding the cell debris, characterized by a low FSC/SSC, using the Beckman Coulter flow cytometer (Coulter Epics XL/Xl-MCL, USA and System II Software, Version 3.0).

Assessment of DNA damage by neutral comet assay. DNA strand breaks in WISH cells after 24 h of exposure with varying concentrations (20 to 100 μg/ml) of $ZnFe_2O_4$-NPs were quantified by neutral comet assay following the method described by Saquib et al. (2012a). In brief, the cells at a density of 6.0×10^4 cells/well were exposed to varying concentrations of $ZnFe_2O_4$-NPs in a 12 well plate for 6 h at 37 °C. The cells were washed with serum free medium and harvested by adding 0.065% trypsin and incubated at 37 °C. The cell suspension was centrifuged at 3000 rpm for 5 min and the pellet was resuspended in 100 μl of PBS. The cells were mixed with 100 μl of 1% LMA and layered on one-third frosted slides, precoated with NMA (1% in PBS) and kept at 4 °C for 10 min. After gelling, another layer of 90 μl of LMA (0.5% in PBS) was added. The cells were lysed in a lysing solution for overnight. After washing with TBE buffer, the slides were subjected to neutral electrophoresis in cold TBE (Tris-base, 90 mM; boric acid, 90 mM; Na_2EDTA, 2.5 mM) buffer. Electrophoresis was performed at 1 V/cm for 30 min (16 mA, 32 V) at 4 °C. All preparative steps were conducted in dark to prevent secondary DNA damage. Each slide was stained with 75 μl of 20 μg/ml ethidium bromide solution for 5 min. The slides were analyzed at 40× magnification (excitation wavelength of 515–560 nm and emission wavelength of 590 nm) using a fluorescence microscope (Nikon Eclipse 80i, Japan) coupled with a charge coupled device (CCD) camera. Images from 50 cells (25 from each replicate slide) were randomly selected and subjected to image analysis using software Comet Assay IV (Perceptive Instruments, Suffolk, UK).

Western blotting. WISH cells treated with $ZnFe_2O_4$-NPs (100 μg/ml) for 72 h at the density of 300,000 cells/well were analyzed for *p53*, *caspase 3*, *bax* and *bcl* 2 proteins by western blotting. In brief, the cell lysis was done by 1× SDS buffer (62.5 mM Tris–HCl, 2% SDS, 10% glycerol, 50 mM DTT) and protein were transferred to polyvinylidene difluoride membranes (Millipore Corporation, Billerica, MA). Primary antibodies including anti-*p53*, anti-*caspase-3*, anti-*bax*, anti-*bcl 2* and anti-*GAPDH*, and secondary antibody (goat anti-rabbit immunoglobulin) labeled with peroxidase (Santa Cruz Biotechnology Inc., Santa Cruz, CA, USA) were used at 1:500 and 1:5000 dilutions, respectively. Immunodetection of proteins was done using the colorimetric method with 1× TMB (3,3′,5,5′-tetramethylbenzidine) H_2O_2 substrate solution (GeNei™, India). Equal protein loading was verified by probing with the anti-*GAPDH* antibody. Densitometric analysis of bands was done using image processing and analysis in Java (ImageJ), free software available from National Institute of Health (http://rsbweb.nih.gov/ij/).

Isolation of total RNA and real-time PCR (qPCR). Total RNA was purified from 3×10^5 cells/well of untreated control and cells treated with $ZnFe_2O_4$-NPs (100 μg/ml) for 72 h using the iPrep™ PureLink™ kit (Invitrogen, USA) by Invitrogen® automated system following the manufacturer's protocol. Purity of total RNA was verified by use of a Nanodrop 8000 spectrophotometer (Thermo Scientific, USA) and the integrity of RNA was visualized on 1% agarose gel using gel documentation system (Universal Hood II, BioRad, USA). The first-strand cDNA synthesis was performed with 1 μg of total RNA and 100 ng of oligo-$p(dT)_{12-18}$ primer and MLV reverse transcriptase (GE Health Care, UK) according to the manufacturer's recommendations. The following sets of specific primers were employed for amplification of each cDNA: *p53* (5′ F-CCCAGCCAAAGAAGAAACCA-3′, 5′R-TTCCAAGGCCTCATTCAGCT-3′), *caspase 3* (5′F-ACATGGCGTGTCATAAAATACC-3′, 5′R-CACAAAGC GACTGGATGAAC-3′), *bax* (5′F-TGCTTCAGGGTTTCATCCAG-3′, 5′R-GG CGGCAATCATCCTCTG-3′), *bcl* 2 (5′F-AGGAAGTGAACATTTCGGTGAC-3′, 5′R-GCTCAGTTCCAGGACCAGGC-3′) and *GAPDH* 5′F-CCACTCCTCCACC TTTGAC-3′, 5′R-ACCCTGTTGCTGTAGCCA-3′. Expression levels were normalized to *GAPDH* gene expression, which was used as an internal housekeeping control. Real-time quantification was performed in the LightCycler® 480 instrument with 96-well plate (Roche Diagnostics, Rotkreuz, Switzerland) using LightCycler®480 SYBR Green I Master (Cat # 04707516001, Roche Diagnostics, Switzerland). PCR mixtures (final volume of 20 μl) contained 10 μl of qPCR GreenMaster, 2.5 μl of 100 ng of the cDNA and 7.5 μM of each primer. Cycling conditions included an initial heat-denaturing step at 95 °C (ramp rate 4.4 °C/s) for 10 min, 45 cycles at 95 °C for 20 s (ramp rate 4.4 °C/s), annealing at 58 °C for all the primers for 20 s (ramp rate 2.2 °C/s), and product elongation and signal acquisition (single mode) at 72 °C for 20 s (ramp rate 4.4 °C/s). Water was used as the template for negative control amplifications included with each PCR run. Serial dilutions of each cDNA (10^{-1}–10^{-6}) were used to generate a quantitative PCR standard curve to calculate the corresponding PCR efficiencies. Results were obtained from three subsamples and PCR was repeated twice per sample. *GAPDH* was used as an internal housekeeping control and its expression was used to normalize the expressions of *p53*, *caspase 3*, *bax* and *bcl 2* genes.

$ZnFe_2O_4$-NPs induced transcriptional analysis by quantitative RT-PCR array. Changes in the relative gene expression of 84 genes responsible for human stress and toxicity pathway were quantified using RT^2 Profiler™ PCR Array (Cat. no. PAHS-003 A; SABiosciences Corporation, Frederick, MD) in a 96-well array format following 72 h exposure of WISH cells to 100 μg/ml of $ZnFe_2O_4$-NPs. cDNA equivalent to 1 μg of total RNA was used for each array. The arrays were run on Roche® LightCycler® 480 (96-well block) (IN, USA) following the recommended cycling programs. Expression data obtained with $ZnFe_2O_4$-NPs treatment group were normalized to the average Ct value of five housekeeping genes (*B2M*, *HPRT1*, *RPL13A*, *GAPDH* and *ACTB*) and expressed with respect to the untreated control. RT-PCR array data were evaluated from at least three independent experiments. The resultant $^{\Delta}$Ct values were combined to calculate the average fold regulation values. Genes that were significantly different for $ZnFe_2O_4$-NPs *versus* the control were determined by a Student's t-test ($p < 0.05$) comparing the $^{\Delta}$Ct values for the triplicate trials for each test sample with the $^{\Delta}$Ct values for the control.

Statistical analysis. Data were expressed as mean ± SD for the values obtained from at least three independent experiments. Statistical analysis was performed by one-way analysis of variance (ANOVA) using Dunnett's multiple comparison test (Sigma Plot 11.0, USA). The level of statistical significance chosen was $p < 0.05$, unless otherwise stated.

Results

Particle characterization by AFM, TEM, zeta (ζ)-potential and DLS measurements

AFM analysis revealed the size of $ZnFe_2O_4$-NPs as 45 nm (Fig. 1A). The TEM analysis of $ZnFe_2O_4$-NPs suggested that the particles were

polyhedral crystallites in the size range of 40–85 nm with the tendency to agglomerate, as shown in Fig. 1B. The ζ-potential values for $ZnFe_2O_4$-NPs in ultrapure water and RPMI were determined to be 0.19 mV and −9.7 mV, respectively (Fig. 1C). The results of hydrodynamic size of the $ZnFe_2O_4$-NPs using DLS provided the average particle size of 56.6 nm in RPMI medium, compared with the much larger particle aggregates of 127 nm in ultrapure water (Fig. 1D).

$ZnFe_2O_4$-NPs induced cytotoxicity and uptake in WISH cells

$ZnFe_2O_4$-NPs were found to be cytotoxic at the concentrations of 80 and 100 μg/ml after 72 h of exposure. At these concentrations, the $ZnFe_2O_4$-NPs induced significant reduction of 17.3 ± 4.3% and 64.4 ± 1.6% in cell viability. However, no apparent evidence of cytotoxicity was noticed after 24 and 48 h of $ZnFe_2O_4$-NPs exposure (data not shown). Similarly, at the lower concentration range of 10 to 60 μg/ml, the $ZnFe_2O_4$-NPs were found to be non-cytotoxic even after 72 h of incubation (Fig. 2A). The decline in the cell viability in NRU assay at concentrations of 60, 80 and 100 μg/ml were determined to be 9.8 ± 2.4%, 15.0 ± 4.8% and 50.7 ± 2.1%, respectively, as compared to the untreated control (Fig. 2A).

Ultrastructural analysis of WISH cells exposed to the greatest concentration of 100 μg/ml for 72 h revealed the localization of $ZnFe_2O_4$-NPs aggregates, in the vesicles and cytoplasm. More than 85% of the analyzed cell sections exhibited internalized $ZnFe_2O_4$-NPs aggregates in treated cells as compared to the untreated controls (Fig. 2B–D).

$ZnFe_2O_4$-NPs induced intracellular ROS generation and changes in ΔΨm

The qualitative data showed an enhanced level of DCF fluorescence in 48 h exposed WISH cells at concentrations of 40 and 60 μg/ml (Fig. 3A). The DCF fluorescence intensity decreased at 80 or 100 μg/ml $ZnFe_2O_4$-NPs, which is attributed to significant cell death at those concentrations (Fig. 3A). Validation of ROS data was done by flow cytometric analysis of $ZnFe_2O_4$-NPs treated WISH cells. Compared to DCF fluorescence (100%) of control, the treatment doses of 20, 40, 60, 80 and 100 μg/ml resulted in 104.5%, 160.7%, 122.3%, 111.0%, and 109.9% and 104.3%, 162.4%, 151.1%, 139.3%, and 119.1% greater ROS generation in WISH cells after 24 and 48 h of incubation, respectively (Fig. 3B). However, the levels of ROS were subdued upon extended exposure to 74 h and were found non-significant. The photomicrograph in Fig. 3C shows the control cells with a sharp fluorescence of

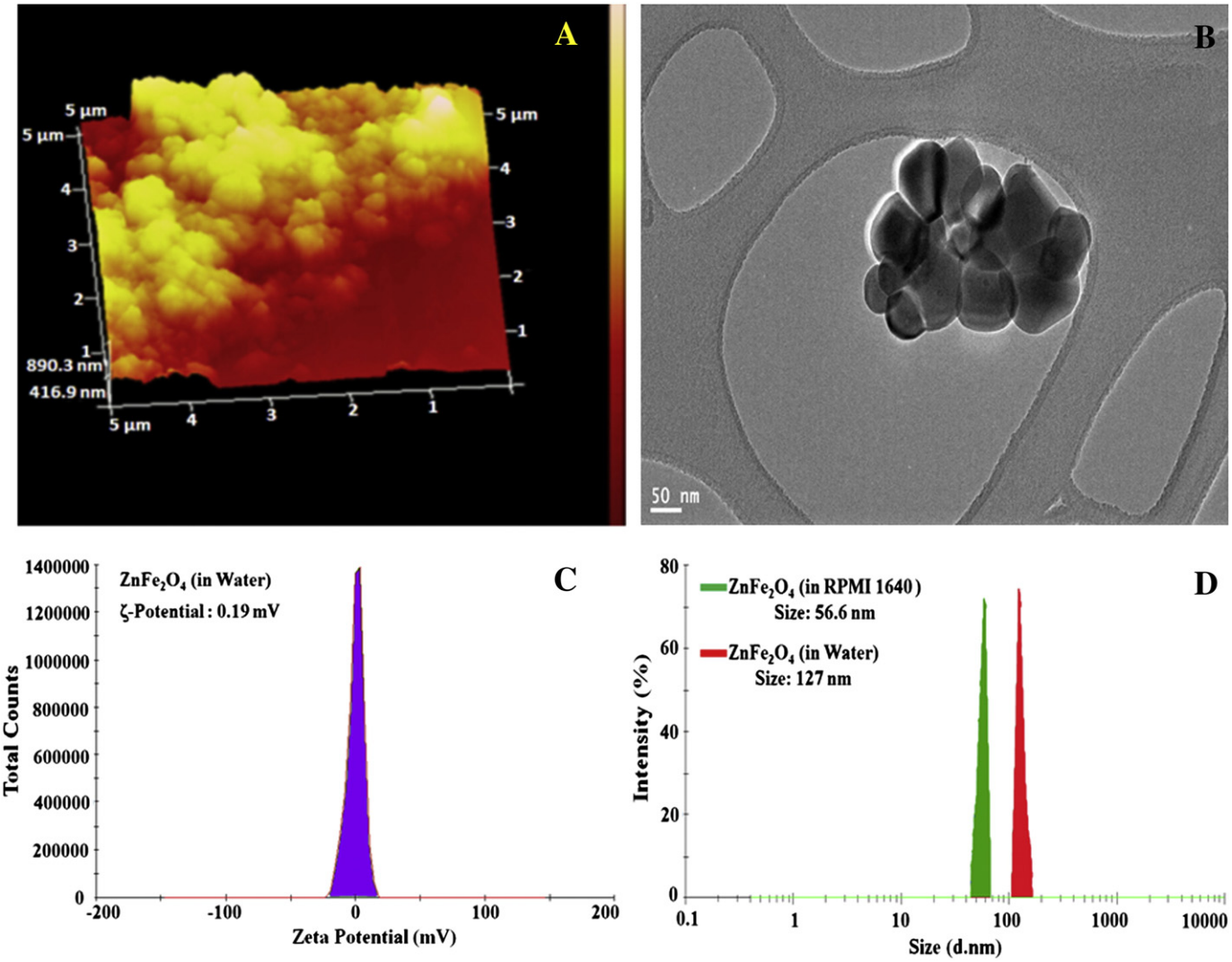

Fig. 1. Particle characterization of $ZnFe_2O_4$-NPs. Depicts the 3D topography of $ZnFe_2O_4$-NPs in an AFM perspective view (panel A). Representative TEM image of $ZnFe_2O_4$-NPs (panel B) at 200,000× magnification. ζ-potential analysis of $ZnFe_2O_4$-NPs suspension in ultrapure water (panel C) and dynamic light scattering (DLS) of $ZnFe_2O_4$-NPs in ultrapure water and RPMI 1640 culture medium (panel D).

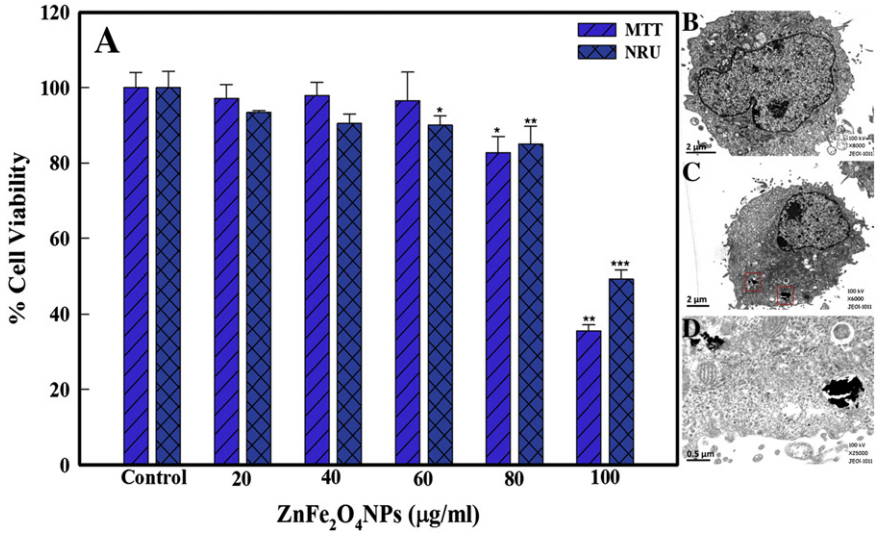

Fig. 2. (A) Cytotoxicity assessment of $ZnFe_2O_4$-NPs in WISH cells exposed for 72 h. Histograms show the percent cell viability using MTT and NRU assays. Data are the mean ± SD of three independent experiments. $^{*}p < 0.05$, $^{**}p < 0.01$, and $^{***}p < 0.001$ *vs.* control. Cells after 72 h exposure to RPMI medium alone (control) and $ZnFe_2O_4$-NPs (100 μg/ml) in RPMI medium were analyzed by TEM. The representative images in panels are depicted as (B) control, (C) $ZnFe_2O_4$-NPs treated at low magnification, and (D) high magnification of boxes showing NPs aggregates in panel C.

Rh123. Nevertheless, the cells treated with 40 to 100 μg/ml of $ZnFe_2O_4$-NPs for 48 h have exhibited a discernable reduction in fluorescence intensity. The flow cytometric data demonstrated 93.6%, 89.8%, 84.7%, 84.8%, and 86.3% and 89.3%, 89.4%, 87.6%, 86.5%, and 90.9% reduction in the $\Delta\Psi m$ of cells treated with 20, 40, 60, 80 and 100 μg/ml of $ZnFe_2O_4$-NPs after 48 and 72 h of incubation (Fig. 3D). Short-term exposure up to 24 h does not exhibit any significant change in $\Delta\Psi m$ of treated cells.

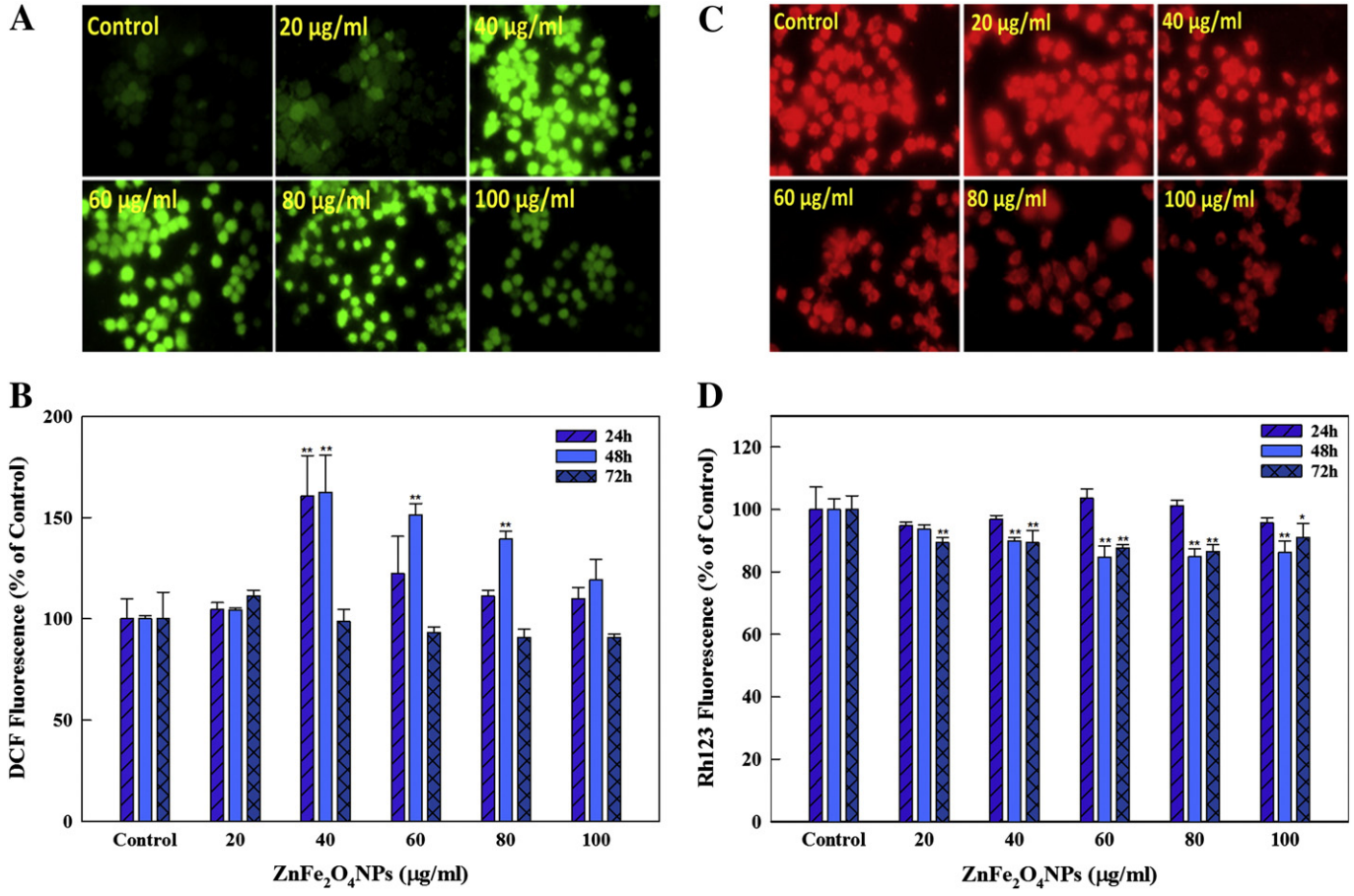

Fig. 3. $ZnFe_2O_4$-NPs mediated intracellular ROS generation. Panel A shows the concentration dependent enhancement in green fluorescence of DCF that occurs in WISH cells due to ROS generation by $ZnFe_2O_4$-NPs exposure for 48 h. Panel B exhibits the comparative analysis of the fluorescence enhancement of DCF obtained by flow cytometry at varying time points with increasing $ZnFe_2O_4$-NPs concentrations. Panel C shows the effect of $ZnFe_2O_4$-NPs on $\Delta\Psi m$ of WISH cells measured in-terms of change in the fluorescence intensity of Rh123 after 48 h. Panel D shows the flow cytometric measurements of $\Delta\Psi m$ in WISH cells at different time periods after exposure with increasing concentrations of $ZnFe_2O_4$-NPs. Each histogram represents the values of mean ± SD of three independent experiments. $^{*}p < 0.05$ and $^{**}p < 0.01$ *vs.* control.

$ZnFe_2O_4$-NPs induced DNA damage

Cultured WISH cells exposed to $ZnFe_2O_4$-NPs for 72 h have exhibited significant induction of DNA damage at the concentrations of 80 and 100 μg/ml. The representative images of DNA damage obtained with the neutral comet assay are shown in Supplementary Fig. 1. The treated cells at these concentrations exhibited 4.0 and 7.4-fold higher OTM values, as compared to the untreated control (Table 1). The frequency distribution analysis suggested the extent of DNA damage in cells treated at the greatest (100 μg/ml) concentration of $ZnFe_2O_4$-NPs almost similar to positive control (EMS, 1 mM) (Supplementary Fig. 2).

Effect of $ZnFe_2O_4$-NPs on cell cycle progression

Cell cycle analysis of propiodium iodide stained control and $ZnFe_2O_4$-NPs treated cells indicated an increase in apoptotic sub-G_1 peak after 48 and 72 h (Fig. 4). A significant increase of 4.4 ± 0.3% and 7.9 ± 0.3%, as well as 7.7 ± 0.4% and 15.2 ± 2.1% ($p < 0.01$) dead cells in sub-G_1 phase appeared with 80 and 100 μg/ml of $ZnFe_2O_4$-NPs treatment for 48 and 72 h, respectively. The proportion of dead cells in the control was found to be 1.2 ± 0.27% and 1.6% ± 0.4 after 48 and 72 h, respectively.

Transcriptional and translational changes in the expression of p53, caspase 3, bax and bcl 2 genes

Compared to untreated control, the expression of tumor suppressor (*p53*), *caspase 3* and pro-apoptotic (*bax*) genes was significantly upregulated to 5.3, 1.6 and 14.9-fold ($p < 0.05$), while the expression of anti-apoptotic (*bcl* 2) gene exhibited 0.18-fold ($p < 0.05$) down regulation in WISH cells treated with 100 μg/ml of $ZnFe_2O_4$-NPs (Fig. 5). The results were further validated by western blot analysis. Compared to the band density of proteins in untreated control, the intensity of bands corresponding to *p53*, *caspase 3* and *bax* proteins in WISH cells, treated with 100 μg/ml of $ZnFe_2O_4$-NPs for 72 h, exhibited an increase of 4.9, 6.5 and 1.5-fold, respectively. However, the anti-apoptotic (*bcl* 2) protein exhibited 0.79-fold lesser protein expression (Fig. 5 inset).

Profiling of gene expression by qPCR array

Effect of $ZnFe_2O_4$-NPs (100 μg/ml) treatment on expression of human stress and toxicity pathway related genes was studied by use of RT^2 Profiler PCR array. Pathway-focused gene expression heat maps showed the upregulation and down-regulation of mRNA transcripts in the range of 3- and 6-folds. Examination of the heat maps suggested strong oxidative or metabolic stress, and induced proinflammatory and heat shock responses upon $ZnFe_2O_4$-NPs treatment. Out of 19 genes for oxidative or metabolic stress, metallothionein 2A (*MT2A*) has exhibited a maximum of 2.0-fold upregulation. Substantial number of genes in this group were down-regulated, and a maximum of 5.8 and 5.6-fold down-regulation has been observed for heme oxygenase (decycling) 1 (*HMOX1*) and cytochrome P450, family 1, subfamily A, polypeptide 1 (*CYP1A1*) genes, respectively. Among the set of 9 genes responsible for inflammation, interleukin 1, beta (*IL-1b*), nuclear factor of kappa light polypeptide gene enhancer in B-cells 1 (*NFKB1*), chemokine (C-C motif) ligand 21 (*CCL21*) and nitric oxide synthase 2, inducible (*NOS2*) have exhibited 2.3, 1.5, 3.7 and 3.0-fold upregulation, respectively. Down-regulation of 2.0-fold has been observed for serpin peptidase inhibitor, clade E (nexin, plasminogen activator inhibitor type 1), and member 1 (*SERPINE1*) gene. Out of 15 heat shock genes, only the heat shock 70 kDa protein 6 (HSP70B′) (*HSPA6*) and heat shock 70 kDa protein 1A (*HSPA1A*) were maximally down-regulated to 136.05 and 2.53-fold, respectively. Among the set of 11 genes for DNA damage and repair, RAD23 homolog A (*Saccharomyces cerevisiae*) (*RAD 23A*), and uracil-DNA glycosylase (*UNG*) have exhibited marginal increase of 1.4

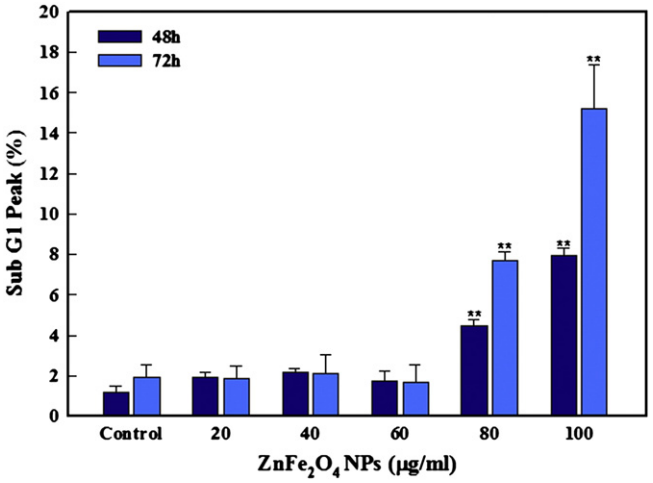

Fig. 4. Effects of $ZnFe_2O_4$-NPs on the percentage of apoptotic cells (mean ± SD). % sub-G_1 peak denotes the percentage of cells with sub diploid DNA content (apoptotic cells) measured in flow cytometric analysis. **$p < 0.01$ *vs.* control.

Table 1
$ZnFe_2O_4$-NPs induced DNA damage in WISH cells, analyzed using different parameters of neutral comet assay.

Groups	Olive tail moment (arbitrary unit)	Tail length (μm)	Tail intensity (%)
Control	0.69 ± 0.11	39.90 ± 3.22	4.15 ± 0.42
EMS (1 mM)	10.16 ± 1.33***	104.67 ± 5.98***	22.03 ± 1.59***
$ZnFe_2O_4$-NPs (μg/ml)			
20	1.31 ± 0.33	39.50 ± 5.61	3.94 ± 0.29
40	1.47 ± 0.31	46.32 ± 6.90	7.71 ± 0.70
60	2.16 ± 0.62	55.52 ± 4.94	9.14 ± 0.72
80	2.77 ± 0.25**	65.39 ± 3.54*	10.06 ± 0.62*
100	5.12 ± 0.44***	76.48 ± 2.59**	16.20 ± 0.75**

Data represent the mean ± SD of three independent experiments done in duplicate; EMS: Ethyl methanesulphonate.
* $p < 0.05$.
** $p < 0.01$.
*** $p < 0.001$.

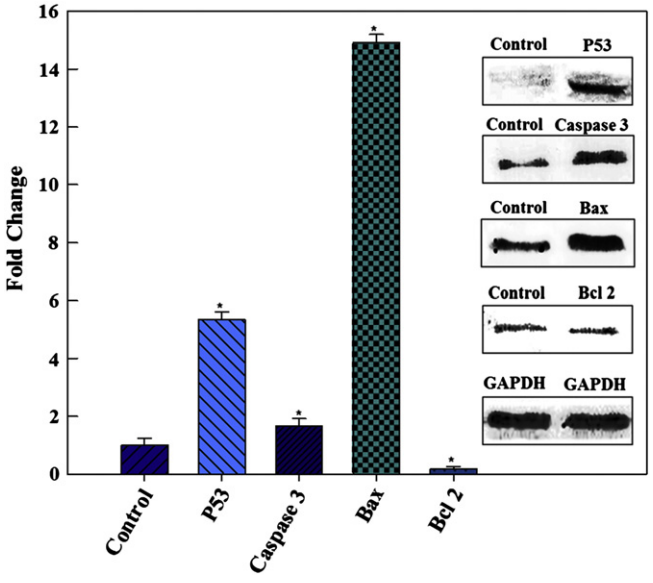

Fig. 5. Transcriptional and translational changes of apoptotic pathway genes in WISH cells. Transcript levels were determined by real-time quantitative PCR. *$p < 0.05$ using one-way ANOVA (Dunnett's multiple comparison test) significantly different when compared to solvent control. Inset shows the western blot protein expression of same apoptotic genes in WISH cells treated with $ZnFe_2O_4$-NPs (100 μg/ml) for 72 h.

and 1.3-fold in expression. Only UDP glucuronosyltransferase 1 family, polypeptide A4 (*UGT1A4*) exhibited a maximum of 2.1-fold down-regulation as compared to the untreated control. Out of 7 genes responsible for growth arrest and senescence, only tumor protein p53 (*TP53*) has exhibited upregulation by 1.3-fold, however, the rest of the genes have exhibited down-regulation of less than 2-fold. Within the apoptosis signaling genes (10 sets), the upregulated genes were BCL2-like 1 (*BCL2L1*) and BCL2-associated X protein (*BAX*), which have exhibited marginal increase of 1.5 and 1.2-fold upregulation. In this group, the tumor necrosis factor receptor superfamily, member 1A (*TNFRSF1A*) has exhibited a maximum of 2.2-fold down-regulation. Genes governing the role in proliferation and carcinogenesis, in particular, cyclin D1 (*CCND1*) has exhibited a maximum of 1.2-fold upregulation, however, gene responsible for early growth response 1 (*EGR1*) has exhibited a maximum down-regulation of 2.5-fold over control (Fig. 6).

Discussion

The spinel ferrite $ZnFe_2O_4$-NPs are used as a contrasting agent in magnetic resonance imaging, routinely utilized for the non-invasive diagnosis and post-therapy assessment of a variety of diseases (Bärcena et al., 2008). There are growing concerns about the possible influence of NPs on human health, and particularly with the exposures during prenatal, pregnancy or early childhood stages (Lacasaña et al., 2005). Several nanosized materials such as carboxylic polystyrene, gold and TiO_2-NPs are reported to cross the placental tissue (Semmler-Behnke et al., 2007; Tian et al., 2009). Uptake of nanosized fluorescently labeled polystyrene beads has been demonstrated across the placental barrier in an *ex-vivo* human placental perfusion model (Wick et al., 2010). Our recent study on TiO_2-NP induced cytotoxicity and DNA damage has also demonstrated the reduction in cell viability, intracellular ROS production, and DNA damage in exposed human amniotic epithelial (WISH) cells (Saquib et al., 2012a). This study has explicitly demonstrated the uptake and accumulation of $ZnFe_2O_4$-NPs in WISH cells, and provided the evidence on the cellular toxicity and related molecular events that trigger cell death of cultured WISH cells upon treatment with $ZnFe_2O_4$-NPs. Generally, the NPs enter into cells through endocytosis and localize in the vacuoles and cell cytoplasm of the exposed cells (Chowdhury et al., 2013; Hussain et al., 2009, 2010). During internalization by endocytosis, the $ZnFe_2O_4$-NPs may undergo degradation/dissolution due to acidic pH of endosomes (Singh et al., 2012), and release Fe ions, which most likely promotes the generation of ROS *via* Haber–Weiss and/or Fenton reactions, and consequently cause oxidative damage in biomolecules (Soenen et al., 2010). Fe ions can also potentially escape into the cytoplasm and become a part of accessible iron ions called the labile iron pool (LIP), which has also been shown to exist in the nucleus (Kruszewski and Iwanenko, 2003; Petrat et al., 2001). Additionally, the large surface area and small size of NPs makes them more compatible for generation of ROS. Our results have demonstrated the potential of $ZnFe_2O_4$-NPs to generate ROS. This observation corroborates with the earlier findings in HepG2, WISH, mouse embryo fibroblast and human lymphoblastoid cell lines, which suggest ROS generation and induction of oxidative stress by NPs (Saquib et al., 2012a; Sharma et al., 2012; Yang et al., 2009; Yin et al., 2010).

Assessment of $ZnFe_2O_4$-NPs cytotoxicity through the MTT and NRU assays exhibited the dose dependent toxic effect on cell viability at concentrations of 60, 80 and 100 μg/ml after 72 h. Our MTT and NRU data is in agreement with the recent reports on TiO_2 and ZnO-NPs induced loss

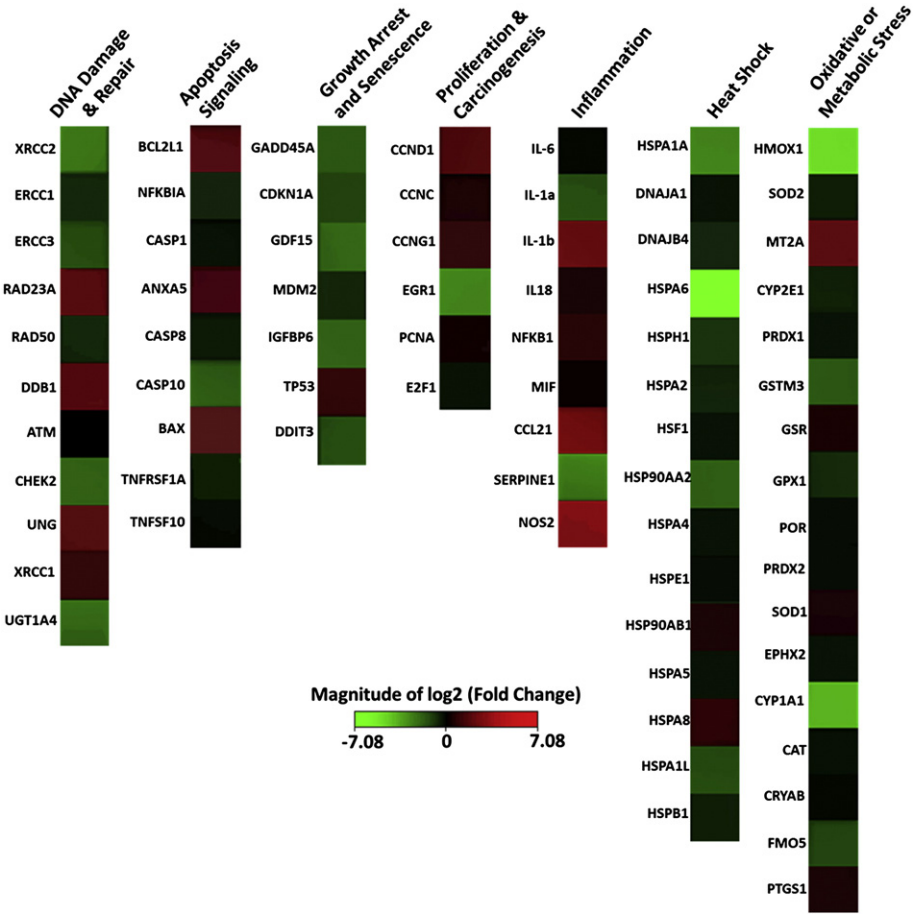

Fig. 6. qPCR array of oxidative stress and toxicity pathway genes in WISH cells. Relative gene expression of 84 genes responsible for human stress and toxicity pathway in $ZnFe_2O_4$-NPs (100 μg/ml) treated WISH cells after 72 h of exposure.

of mitochondrial potential and lysosomal membrane destabilization (Hussain et al., 2010; Saquib et al., 2012a; Sharma et al., 2012). Alterations in mitochondrial activity, based on cationic fluorescent probe Rh123, indicated the role of oxidative stress in toxicity of $ZnFe_2O_4$-NPs. The lesser fluorescence intensity of Rh123 indicates perturbation of inner mitochondrial membranes, and consequently mitochondrial dysfunction as a result of ROS. The flow cytometric analysis of 48 and 72 h treated WISH cells also exhibited the activation of apoptosis process with discernible appearance of subG1 peaks at higher $ZnFe_2O_4$-NPs concentrations. The translational data on modulation of *bax*/*bcl* 2 ratio and release of *caspase 3* have strengthened the role of $ZnFe_2O_4$-NPs in inducing mitochondrial dependent apoptotic pathway. In general, the caspases are crucial for the activation and execution of apoptosis. The main intrinsic pathway is characterized by mitochondrial dysfunction, with the release of *cytochrome c*, activation of *caspase 9*, and subsequently of *caspase 3* (Porter and Jänicke, 1999). Activation of *caspase 3* is considered to be the "point-of-no-return" in the apoptotic signaling cascade (Green and Amarante-Mendes, 1998). Typically, *p53* is activated when DNA damage occurs or cells are stressed and *p53* is translocated to the nucleus, where it can induce proapoptotic gene expression on the mitochondrial membrane and activate the effector caspases and accelerate cell death (Levine, 1997; Sheikh and Fornace, 2000). Our translational and transcriptional studies reaffirmed the potential of $ZnFe_2O_4$-NPs to induce apoptotic pathway. The western blot and qPCR data are in accordance with the recent reports on nickel ferrite and silica NPs inducing apoptotic pathway genes in A549 and HepG2 cells (Ahamed et al., 2011; Ahmad et al., 2012).

To better understand the dynamics of cellular responses upon $ZnFe_2O_4$-NPs exposure, a comprehensive analysis of toxicity and stress pathways was performed in WISH cells. We analyzed the gene expression of 84 genes, reportedly involved in seven specific cellular stress-responsive pathways *viz.* oxidative or metabolic stress, DNA damage and repair, growth arrest and senescence, apoptosis signaling, proliferation and carcinogenesis, inflammation and heat shock. The toxicogenomic data analysis revealed increased levels of transcripts, encoding for proinflammatory cytokine IL-1b mRNA. Our data on the elevated expression level of inflammatory genes in WISH cells upon $ZnFe_2O_4$-NPs exposure correspond well with the recent report on the endothelial dysfunction and inflammation induced by iron oxide nanoparticles (Fe_2O_3 and Fe_3O_4) in human aortic endothelial cells (HAECs) and monocyte (U937 cells) (Zhu et al., 2011). Also, the upregulation of NF-kappa-B1 (*NFKB1*) gene was observed in $ZnFe_2O_4$-NPs treated WISH cells, which is essential for inflammation, immunity, and cell proliferation (Wu et al., 2010). Furthermore, the upregulation of chemokine (C-C motif) ligand 21 (*CCL21*) genes in this study clearly suggested that $ZnFe_2O_4$-NPs activate the translocation of *NFKB* complex to nucleus and upregulate the expression of chemokine (*CCL21*) genes in WISH cells. The results also exhibited higher expression of inducible nitric oxide synthase (*NOS2*) genes in $ZnFe_2O_4$-NPs exposed WISH cells. The increased expression of *NOS2* genes is one of the hallmarks of inflammatory responses to a variety of stimuli, including lipopolysaccharides, metals, and oxidative stress (Lee et al., 2012). Our data on *NOS2* expression is in line with a recent report on multi-walled carbon nanotubes, exhibiting the induction of *NOS2* in mouse RAW264.7 macrophages (Lee et al., 2012). The $ZnFe_2O_4$-NPs treated cells have also exhibited enhanced expression of metallothionein 2A (*MT2A*) gene, which corroborates with the increased expression of *MT2A* genes in HeLa and normal human lung fibroblast (IMR-90) cells treated with silver NPs (AshaRani et al., 2009; Xu et al., 2012). Interestingly, the *HMOX1* and *CYP1A1* genes exhibited down-regulation, and a similar response has been reported in mice instilled with low organic carbon and ultrafine carbon particles (Stoeger et al., 2009). *HMOX1* gene product protects the cells from detrimental effects of oxidants through the reduction of pro-oxidant heme and liberation of bilirubin, a potent ROS scavenger (Maines and Gibbs, 2005). However, there are contradictory reports on the expression of *HMOX1* gene under conditions of oxidative stress. Bolati et al. (2013) have demonstrated the down regulation of *HMOX1* gene expression, and increased 8-OHdG levels in kidney of indoxyl sulfate (uremic toxin) treated rats under condition of elevated ROS levels. This has been attributed to the (i) toxin-induced *NFKB* activation that inhibits nuclear factor (*Nrf2*)-antioxidant response element (ARE); and (ii) upregulation of *p53* expression, which may binds to ARE sequences, and thereby, interferes with the interaction of *Nrf2* and ARE sequences. Our results also exhibiting the activation of *NFKB1* and *p53* expression in $ZnFe_2O_4$-NPs treated cells support the role of similar mechanism in down regulation of *HMOX1* expression by interfering with the interaction between *Nrf2* and ARE sequences at increased ROS levels in WISH cells. Moreover, Alba et al. (2008) have also reported the *HMOX1* down regulation under higher ROS levels in human neutrophils treated with angiotensin II (Ang II), a known inducer to promote ROS, which suggests that *HMOX1* expression is not solely dependent on ROS status in cells.

Similarly, Gharavi and El-Kadi (2005) have suggested *CYP1A1* down-regulation by the proinflammatory cytokines interleukin 1β (*Il-1β*), *IL-6*, and tumor necrosis factor α in an aryl hydrocarbon receptor-dependent manner in murine hepatoma cell lines. Consistent with these findings, our data also showed the upregulation of proinflammatory gene *IL-1b* upon $ZnFe_2O_4$-NPs exposure, and down-regulation of *CYP1A1* gene in WISH cells. In addition, $ZnFe_2O_4$-NPs exposure also resulted in down regulation of *UGT1A4* and *EGR1* genes in WISH cells. Multi-walled carbon nanotubes and gold ions are reported to down-regulate the expression of *EGR1* in human skin fibroblasts and macrophages (Ding et al., 2005; Seifert et al., 2012). It is reported that the down-regulation of *EGR1* is associated with upregulation of chemokines (Gersten et al., 2009). The data also exhibited 3.7-fold higher expression of the chemokine *CCL21* gene, with down-regulation of *EGR1* gene in $ZnFe_2O_4$-NPs treated WISH cells.

Conclusions

This study provides the first evidence of cyto- and genotoxicity of $ZnFe_2O_4$-NPs in human amnion epithelial (WISH) cell line. Significant reduction of $\Delta\Psi m$ and increased intracellular ROS generation suggested the role of these NPs in inducing oxidative stress leading to DNA damage in treated cells. The results elucidated that $ZnFe_2O_4$-NPs trigger apoptosis and/or necrosis in WISH cells through mitochondria dependent intrinsic apoptotic pathway. Transcriptome analysis of 84 genes revealed the upregulation of inflammatory (*IL1b*, *NFKB1*, *CCL21* and *NOS2*), metallothionein (*MTA2A*) and down-regulation of oxidative (*HMOX1* and *CYP1A1*), DNA damage (*UGT1A4*) and early growth response (*EGR1*) genes in $ZnFe_2O_4$-NPs treated WISH cells. It is contemplated that the extrapolation of *in vitro* dose response data to *in vivo* situation, *i.e.*, in placenta or embryo is still a challenge. Therefore, further studies are warranted to investigate the particokinetics and rate of transport of $ZnFe_2O_4$-NPs in amniotic cells to ascertain more realistic NP induced toxicity and risk assessment.

Supplementary data to this article can be found online at http://dx.doi.org/10.1016/j.taap.2013.09.001.

Conflict of interest

There is no conflict of interest.

Acknowledgments

Financial support through the National Plan for Sciences and Technology (NPST Project No. 10-NAN1115-02, NPST Project No. 10-ENV-1314-02) and Chair for DNA research, King Saud University, Riyadh, for this study, is greatly acknowledged. JM is also grateful to the Visiting Professor Program, King Saud University for all support to carry out this collaborative research.

References

Ahamed, M., Akhtar, M.J., Siddiqui, M.A., Ahmad, J., Musarrat, J., Al-Khedhairy, A.A., AlSalhi, M.S., Alrokayan, S.A., 2011. Oxidative stress mediated apoptosis induced by nickel ferrite nanoparticles in cultured A549 cells. Toxicology 283, 101–108.

Ahmad, J., Ahamed, M., Akhtar, M.J., Alrokayan, S.A., Siddiqui, M.A., Musarrat, J., Al-Khedhairy, A.A., 2012. Apoptosis induction by silica nanoparticles mediated through reactive oxygen species in human liver cell line HepG2. Toxicol. Appl. Pharmacol. 259, 160–168.

Alba, G., El Bekay, R., Chacón, P., Reyes, M.E., Ramos, E., Oliván, J., Jiménez, J., López, J.M., Martín-Nieto, J., Pintado, E., Sobrino, F., 2008. Heme oxygenase-1 expression is down-regulated by angiotensin II and under hypertension in human neutrophils. J. Leukoc. Biol. 84, 397–405.

AshaRani, P., Hande, M.P., Valiyaveettil, S., 2009. Anti-proliferative activity of silver nanoparticles. BMC Cell Biol. 10, 65.

Bärcena, C., Sra, A.K., Chaubey, G.S., Khemtong, C., Liu, J.P., Gao, J., 2008. Zinc ferrite nanoparticles as MRI contrast agents. Chem. Commun. 19, 2224–2226.

Bolati, D., Shimizu, H., Yisireyili, M., Nishijima, F., Niwa, T., 2013. Indoxyl sulfate, a uremic toxin, downregulates renal expression of Nrf2 through activation of NF-κB. BMC Nephrol. 14, 56.

Chowdhury, S.M., Lalwani, G., Zhang, K., Yang, J.Y., Neville, K., Sitharaman, B., 2013. Cell specific cytotoxicity and uptake of graphene nanoribbons. Biomaterials 34, 283–293.

Di Guglielmo, C., López, D.R., De Lapuente, J., Mallafre, J.M.L., Suàrez, M.B., 2010. Embryotoxicity of cobalt ferrite and gold nanoparticles: a first *in vitro* approach. Reprod. Toxicol. 30, 271–276.

Ding, L.H., Shingyoji, M., Chen, F., Hwang, J.J., Burma, S., Lee, C., Cheng, J.F., Chen, D.J., 2005. Gene expression profiles of normal human fibroblasts after exposure to ionizing radiation: a comparative study of low and high doses. Radiat. Res. 164, 17–26.

Dwivedi, S., Al-Khedhairy, A.A., Ahamed, M., Musarrat, J., 2013. Biomimetic synthesis of selenium nanospheres by bacterial strain JS-11 and its role as a biosensor for nanotoxicity assessment: a novel Se-bioassay. PLoS One 8 (3), e57404.

Gersten, M., Alirezaei, M., Marcondes, M.C.G., Flynn, C., Ravasi, T., Ideker, T., Fox, H.S., 2009. An integrated systems analysis implicates EGR1 downregulation in SIVE-induced neural dysfunction. J. Neurosci. 29, 12467–12476.

Gharavi, N., El-Kadi, A.O., 2005. Down-regulation of aryl hydrocarbon receptor-regulated genes by tumor necrosis factor-alpha and lipopolysaccharide in murine hepatoma Hepa 1c1c7 cells. J. Pharm. Sci. 94, 493–506.

Green, D.R., Amarante-Mendes, G.P., 1998. The point of no return: mitochondria, caspases, and the commitment to cell death. Results Probl. Cell Differ. 24, 45–61.

http://rsbweb.nih.gov/ij/ (Assessed on May 20, 2013).

Hussain, S., Boland, S., Baeza-Squiban, A., Hamel, R., Thomassen, L.C.J., Martens, J.A., Billon-Galland, M.A., Fleury-Feith, J., Moisan, F., Pairon, J.C., Marano, F., 2009. Oxidative stress and proinflammatory effects of carbon black and titanium dioxide nanoparticles: role of particle surface area and internalized amount. Toxicology 260, 142–149.

Hussain, S., Thomassen, L., Ferecatu, I., Borot, M.C., Andreau, K., Martens, J., Fleury, J., Baeza-Squiban, A., Marano, F., Boland, S., 2010. Carbon black and titanium dioxide nanoparticles elicit distinct apoptotic pathways in bronchial epithelial cells. Part. Fibre Toxicol. 7, 10.

Kruszewski, M., Iwaneńko, T., 2003. Labile iron pool correlates with iron content in the nucleus and the formation of oxidative DNA damage in mouse lymphoma L5178Y cell lines. Acta Biochim. Pol. 50, 211–215.

Kumar, C.S.S.R., 2006. Nanomaterials—Toxicity, Health and Environmental Issues. Wiley-VCH Verlag GmbH & Co KGaA, Weinheim, Germany.

Kumar, D., Lundgren, D.W., Moore, R.M., Silver, R.J., Moore, J.J., 2004. Hydrogen peroxide induced apoptosis in amnion-derived WISH Cells is not inhibited by vitamin C. Placenta 25, 266–272.

Lacasaña, M., Esplugues, A., Ballester, F., 2005. Exposure to ambient air pollution and prenatal and early childhood health effects. Eur. J. Epidemiol. 20, 183–199.

Lee, J.K., Sayers, B.C., Chun, K., Lao, H., Shipley-Phillips, J.K., Bonner, J.C., Langenbach, R., 2012. Multi-walled carbon nanotubes induce COX-2 and iNOS expression via MAP kinase-dependent and -independent mechanisms in mouse RAW264.7 macrophages. Part. Fibre Toxicol. 9, 14.

Levine, A.J., 1997. p53, the cellular gatekeeper for growth and division. Cell 88, 323–331.

Lundgren, D.W., Moore, R.M., Collins, P.L., Moore, J.J., 1997. Hypotonic stress increases cyclooxygenase-2 expression and prostaglandin release from amnion-derived WISH cells. J. Biol. Chem. 272, 20118–20124.

Maines, M.D., Gibbs, P.E.M., 2005. 30 some years of heme oxygenase: from a "molecular wrecking ball" to a "mesmerizing" trigger of cellular events. Biochem. Biophys. Res. Commun. 338, 568–577.

Marmorato, P., Ceccone, G., Gianoncelli, A., Pascolo, L., Ponti, J., Rossi, F., Salomé, M., Kaulich, B., Kiskinova, M., 2011. Cellular distribution and degradation of cobalt ferrite nanoparticles in Balb/3T3 mouse fibroblasts. Toxicol. Lett. 207, 128–136.

Moore, R.M., Lundgren, D.W., Silver, R.J., Moore, J.J., 2002. Lactosylceramide-induced apoptosis in primary amnion cells and amnion-derived WISH cells. J. Soc. Gynecol. Investig. 9, 282–289.

Petrat, F., de Groot, H., Rauen, U., 2001. Subcellular distribution of chelatable iron: a laser scanning microscopic study in isolated hepatocytes and liver endothelial cells. Biochem. J. 356, 61–69.

Porter, A.G., Jänicke, R.U., 1999. Emerging roles of caspase-3 in apoptosis. Cell Death Differ. 6, 99–104.

Prithviraj Swamy, P.M., Basavaraja, S., Lagashetty, A., Srinivas Rao, N.V., Nijagunappa, R., Venkataraman, A., 2011. Synthesis and characterization of zinc ferrite nanoparticles obtained by self-propagating low-temperature combustion method. Bull. Mater. Sci. 34, 1325–1330.

Saquib, Q., Al-Khedhairy, A.A., Siddiqui, M.A., Abou-Tarboush, F.M., Azam, A., Musarrat, J., 2012a. Titanium dioxide nanoparticles induced cytotoxicity, oxidative stress and DNA damage in human amnion epithelial (WISH) cells. Toxicol. *In Vitro* 26, 351–361.

Saquib, Q., Musarrat, J., Siddiqui, M.A., Dutta, S., Dasgupta, S., Giesy, J.P., Al-Khedhairy, A.A., 2012b. Cytotoxic and necrotic responses in human amniotic epithelial (WISH) cells exposed to organophosphate insecticide phorate. Mutat. Res. 744, 125–134.

Semmler-Behnke, M., Fertsch, S., Schmid, G., Wenk, A., Kreyling, W.G., 2007. Uptake of 1.4 nm versus 18 nm gold nanoparticles in secondary target organs is size dependent in control and pregnant rats after intratrecheal or intravenous application. EuroNanoForum 2007—Nanotechnology in Industrial Applications. European Communities, Luxembourg, pp. 102–104.

Seifert, O., Matussek, A., Sjögren, F., Geffers, R., Anderson, C.D., 2012. Gene expression profiling of macrophages: implications for an immunosuppressive effect of dissolucytotic gold ions. J. Inflamm. 9, 43.

Sharma, V., Anderson, D., Dhawan, A., 2012. Zinc oxide nanoparticles induce oxidative DNA damage and ROS-triggered mitochondria mediated apoptosis in human liver cells (HepG2). Apoptosis 17, 852–870.

Sheikh, M.S., Fornace, A.J., 2000. Role of p53 family members in apoptosis. J. Cell. Physiol. 182, 171–181.

Singh, N., Jenkins, G.J.S., Nelson, B.C., Marquis, B.J., Maffeis, T.G.G., Brown, A.P., Williams, P.M., Wright, C.J., Doak, S.H., 2012. The role of iron redox state in the genotoxicity of ultrafine superparamagnetic iron oxide nanoparticles. Biomaterials 33, 163–170.

Soenen, S.J.H., Himmelreich, U., Nuytten, N., Pisanic, T.R., Ferrari, A., De Cuyper, M., 2010. Intracellular nanoparticle coating stability determines nanoparticle diagnostics efficacy and cell functionality. Small 6, 2136–2145.

Stoeger, T., Takenaka, S., Frankenberger, B., Ritter, B., Karg, E., Maier, K., Schulz, H., Schmid, O., 2009. Deducing in vivo toxicity of combustion-derived nanoparticles from a cell-free oxidative potency assay and metabolic activation of organic compounds. Environ. Health Perspect. 117, 54–60.

Tantra, R., Knigh, T.A., 2011. Cellular uptake and intracellular fate of engineered nanoparticles: a review on the application of imaging techniques. Nanotoxicology 5, 381–392.

Tian, F., Razansky, D., Estrada, G.G., Semmler-Behnke, M., Beyerle, A., Kreyling, W., Ntziachristos, V., Stoeger, T., 2009. Surface modification and size dependence in particle translocation during early embryonic development. Inhal. Toxicol. 21, 92–96.

Vochita, G., Creanga, D., Focanici-Ciurlica, E.L., 2012. Magnetic nanoparticle genetic impact on root tip cells of sunflower seedlings. Water Air Soil Pollut. 223, 2541–2549.

Wick, P., Malek, A., Manser, P., Meili, D., Maeder-Althaus, X., Diener, L., Diener, P.A., Zisch, A., Krug, H.F., von Mandach, U., 2010. Barrier capacity of human placenta for nanosized materials. Environ. Health Perspect. 118, 432–436.

Wu, W., Samet, J.M., Peden, D.B., Bromberg, P.A., 2010. Phosphorylation of p65 is required for zinc oxide nanoparticle-induced interleukin 8 expression in human bronchial epithelial cells. Environ. Health Perspect. 118, 982–987.

Xiao-Feng, P., Ting, Q., 2010. Proceedings of the Bioinformatics and Biomedical Engineering (iCBBE), 2010 4th International Conference: 18–20 June 2010; China, pp. 1–4 (Available at: http://ieeexplore.ieee.org/stamp/stamp.jsp?tp=&arnumber=5518295&tag=1. Assessed on May 20, 2013).

Xu, L., Li, X., Takemura, T., Hanagata, N., Wu, G., Chou, L.L., 2012. Genotoxicity and molecular response of silver nanoparticle (NP)-based hydrogel. J. Nanobiotechnol. 10, 16.

Yang, H., Liu, C., Yang, D., Zhang, H., Xi, Z., 2009. Comparative study of cytotoxicity, oxidative stress and genotoxicity induced by four typical nanomaterials: the role of particle size, shape and composition. J. Appl. Toxicol. 29, 69–78.

Yin, H., Too, H.P., Chow, G.M., 2005. The effects of particle size and surface coating on the cytotoxicity of nickel ferrite. Biomaterials 26, 5818–5826.

Yin, H., Casey, P.S., McCall, M.J., Fenech, M., 2010. Effects of surface chemistry on cytotoxicity, genotoxicity, and the generation of reactive oxygen species induced by ZnO nanoparticles. Langmuir 26, 15399–15408.

Zhao, Y., Nalwa, H., 2007. Nanotoxicology—Interactions of Nanomaterials With Biological Systems. American Scientific Publishers, California, USA.

Zhao, F., Zhao, Y., Liu, Y., Chang, X., Chen, C., Zhao, Y., 2011. Cellular uptake, intracellular trafficking, and cytotoxicity of nanomaterials. Small 7, 1322–1337.

Zhu, M., Wang, B., Wang, Y., Yuan, L., Wang, H., Wang, M., Ouyang, H., Chai, Z., Feng, W., Zhao, Y., 2011. Endothelial dysfunction and inflammation induced by iron oxide nanoparticle exposure: risk factors for early atherosclerosis. Toxicol. Lett. 203, 162–171.